Monthly Notices of the ROYAL ASTRONOMICAL SOCIETY

MNRAS **544,** 283–292 (2025) https://doi.org/10.1093/mnras/staf1734
Advance Access publication 2025 October 13

Exploring cyanopolyynes towards the C-rich post-AGB star IRAS 22272+5435

Yuxuan Sun [1,2] Xiaohu Li,[1,3,4★] Mirek R. Schmidt,[5] Ryszard Szczerba,[1,3,5] Tom J. Millar [6] Jixian Sun,[7,8] Juan Tuo,[1,3] Yong Zhang [1,9,10] Gleb Fedoseev [1,3] Chuanlu Yang,[1,11] Tao Yang,[3,12,13] Wasim Iqbal,[1,3] Jixing Ge,[1,3] Yanan Feng,[14] Xiaomin Song,[1,2] Yihan Wu,[1,3] Xia Zhang,[1,3] Zhenzhen Miao,[1,3] Fangfang Li,[1,2,3] Rong Ma,[1,3] Xuan Fang,[1,10,15,16] Zhiping Kou[1,2] and Jianchao Yang[2,17]

[1]*Xinjiang Astronomical Observatory, Chinese Academy of Sciences, 150 Science 1-Street, Urumqi, Xinjiang 830011, China*
[2]*University of Chinese Academy of Sciences, Beijing 100049, China*
[3]*Xinjiang Key Laboratroy of Radio Astrophysics, 150 Science 1-Street, Urumqi, Xinjiang 830011, China*
[4]*State Key Laboratory of Radio Astronomy and Technology, A20 Datun Road, Beijing 100101, China*
[5]*Nicolaus Copernicus Astronomical Center, Rabiańska 8, PL-87-100 Toruń, Poland*
[6]*Astrophysics Research Centre, School of Mathematics and Physics, Queen's University Belfast, Belfast BT7 1NN, UK*
[7]*Purple Mountain Observatory, Chinese Academy of Sciences, Nanjing, Jiangsu 210034, China*
[8]*Key Laboratory of Radio Astronomy, Chinese Academy of Sciences, Nanjing, Jiangsu 210034, China*
[9]*School of Physics and Astronomy, Sun Yat-sen University, Zhuhai, Guangdong 510275, China*
[10]*Laboratory for Space Research, Faculty of Science, The University of Hong Kong, Hong Kong 999077, China*
[11]*School of Physics and Optoelectronic Engineering, Ludong University, Yantai, Shandong 264025, China*
[12]*State Key Laboratory of Precision Spectroscopy, East China Normal University, Shanghai 200062, China*
[13]*Collaborative Innovation Center of Extreme Optics, Shanxi University, Taiyuan, Shanxi 030006, China*
[14]*College of Physics and Electrical Engineering, Anyang Normal University, Anyang, Henan 455000, China*
[15]*CAS Key Laboratory of Optical Astronomy, National Astronomical Observatories, Chinese Academy of Sciences, Beijing 100101, China*
[16]*School of Astronomy and Space Sciences, University of Chinese Academy of Sciences, Beijing 100049, China*
[17]*Beijing National Laboratory for Molecular Sciences, Institute of Chemistry, Chinese Academy of Sciences, Beijing 100190, China*

Accepted 2025 September 29. Received 2025 September 24; in original form 2025 June 3

ABSTRACT

Cyanopolyynes are a class of long carbon-chain molecules that are widely distributed in interstellar clouds, but their presence in the circumstellar envelopes (CSEs) of evolved stars appears to be limited to only a few well-studied sources. This study aims to search for the presence of cyanopolyynes in the CSE of the C-rich post-asymptotic giant branch (post-AGB) star IRAS 22272+5435 through observational analysis and radiative transfer modelling. Observations were conducted using the Tianma 65 m radio telescope (TMRT) at ∼15 GHz and the Purple Mountain Observatory (PMO) 13.7 m MM-Wave telescope at ∼90 GHz. The HC_3N $J = 10$–9 and HCN $J = 1$–0 transitions were clearly detected in the PMO 13.7 m data, while no significant signals of other cyanopolyynes were detected with TMRT. Based on the observed HC_3N line, we constructed a spherically symmetric non-thermodynamic equilibrium radiative transfer model, extrapolating the abundance distribution structure from the well-studied C-rich AGB star IRC+10216 to IRAS 22272+5435. The model successfully reproduces the observed HC_3N and HCN profiles and predicts the line intensities of HC_5N and HC_7N. Although the results suggest that these heavier cyanopolyynes may be present in the CSE, their detections are hindered by the large distance and significant beam dilution effects. This study provides valuable observational constraints and theoretical insights into the formation and evolution of carbon-chain molecules in post-AGB environments.

Key words: astrochemistry – stars: AGB and post-AGB – circumstellar matter – ISM: molecules.

1 INTRODUCTION

After experiencing a phase of intense mass loss (10^{-8}–10^{-4} $M_\odot$ yr^{-1}) (E. De Beck et al. 2010), low- and intermediate-mass stars (∼ 0.8–8$M_\odot$) will terminate their evolution along the asymptotic giant branch (AGB). Then they evolve to a later stage with higher effective temperatures (5000–30 000 K). At this later stage, the circumstellar gas of stars gradually begins to be stripped away. The core temperature rises, and emits a large amount of ultraviolet radiation, which heats and excites the surrounding gas. This phase, known as the post-AGB stage (H. Van Winckel 2003), lasts only a few hundred years as the star transitions towards becoming a planetary nebula. Therefore, only a few hundred of such stars are known in

★ E-mail: xiaohu.li@xao.ac.cn

our Galaxy (R. Szczerba et al. 2007). This is one of the reasons for them being among the least understood phases of stellar evolution. Moreover, AGB stars can be classified into three categories based on the carbon-to-oxygen abundance ratio ([C]/[O]) in their atmospheres: carbon-rich (C-rich) stars ([C]/[O] > 1), oxygen-rich (O-rich) stars ([C]/[O] < 1), and S-type stars ([C]/[O] ≈ 1) (H. Olofsson 1996).

Due to violent mass ejection and low surface gravity, post-AGB stars are typically surrounded by circumstellar envelopes (CSEs). The CSEs of post-AGB stars contain a large amount of organic molecules (S. Kwok 1993). In the circumstellar environment, carbon-chain molecules play a crucial role in driving complex chemical processes, contributing to the formation and evolution of organic compounds in stellar atmospheres (P. Thaddeus & M. McCarthy 2001). Currently, cyanopolyynes ($HC_{2n+1}N$, where $n = 1, 2, 3$, etc.) are a well-studied class of interstellar carbon-chain cyanides, characterized by their simple, linear structure. Their formation in CSEs is closely related to the local carbon-enriched prevailing chemical conditions (T. J. Millar & E. Herbst 1994). For post-AGB stars, the presence of cyanopolyynes indicates reaction pathways in which carbon-chain molecules form longer chains through gradual addition (J. Cernicharo, J. R. Goicoechea & E. Caux 2000). Studying the abundance and distribution of these molecules can help reveal the chemical processes of carbon-chain growth and the mechanisms by which complex molecules gradually form in molecular clouds (L. M. Ziurys 2006).

Over the last several years, interstellar cyanides drew a particular attention from the astronomical society. Since 2020, the discoveries of few dozen new molecules are reported annually. A large fraction of these new molecules comprises a chain of two or more carbon atoms and a CN group (e.g. J. Cernicharo et al. 2020, 2024; C. Xue et al. 2020; M. C. McCarthy et al. 2021). An important breakthrough was the detection of first true individual polyaromatic hydrocarbons (PAHs) in TMC-1 dark cloud (B. A. McGuire et al. 2021; G. Wenzel et al. 2024). It should be noted that all of these individual PAHs are cyanides. The recent laboratory results shows that cyanopolyynes, as well as other carbon-chain species, present in dark clouds may play a key role in the formation of various substituted aliphatic hydrocarbons observed around comet 67P–Churimov–Gerasimenko (G. Fedoseev et al. 2025). This makes cyanopolyynes, as the simplest representatives of carbon-chain molecules and cyanides, an important target for the observation in other regions of the interstellar medium, such as envelopes of C-rich AGB stars.

For C-rich evolved stars, existing studies have focused more on strong emission sources, such as the AGB star IRC+10216 and the post-AGB star CRL 2688. In these two sources, the longest known carbon-chain molecule HC_9N was detected at that time (Truong-Bach, D. Graham & Nguyen-Q-Rieu 1996; X.-Y. Zhang et al. 2017). In addition, cyanopolyynes are also suggested to exist in planetary nebulae, with HC_3N being detected in two young planetary nebulae-NGC 7027 and K4–47, which are approximately 600 and 900 yr old, respectively (Y. Zhang, S. Kwok & Dinh-V-Trung 2008; D. R. Schmidt & L. M. Ziurys 2019). These observations provided new details about chemical inventory of CSEs, and new insights into the formation and evolution of complex organic molecules in these environments.

IRAS 22272+5435, also known as SAO 34504, is a well-known high-luminosity C-rich post-AGB star (L. Začs, V. G. Klochkova & V. E. Panchuk 1995). Its carbon-to-oxygen abundance ratio is estimated to be ∼1.8 (B. E. Reddy et al. 2002) or ∼1.6 (L. Začs et al. 2016), which is relatively high compared to other evolved stars. This G5-type supergiant (B. J. Hrivnak & S. Kwok 1991) is enveloped by a dense circumstellar shell, composed of material ejected during its AGB phase, which it departed ∼400 yr ago (T. Ueta et al. 2001). Its effective temperature is between 5250 to 5750 K (L. Začs et al. 2016), and it exhibits a complex pulsation period of 132 d (B. J. Hrivnak et al. 2013). The star's luminosity, core mass, and radius are 10 990 $L_\odot$, 0.574 $M_\odot$, and 106 $R_\odot$, respectively, and it is located 1.65 kpc away from us (A. Mishra, A. Li & B. W. Jiang 2016). In the CSE of IRAS 22272+5435, several characteristics of dust have been identified, including the infrared emission characteristics of the aromatic compounds mentioned above, as well as unknown features at 21 and 30 μm (R. Szczerba et al. 1997). In particular, emission features of C_2 have been detected in the CSE of this star, with models for these features successfully constructed by M. R. Schmidt et al. (2013). Based on observations from the *Herschel Space Observatory* using the HIFI receiver, transitions of CO and HCN have also been detected (V. Bujarrabal et al. 2012). These findings indicate the presence of a large number of organic molecules in IRAS 22272+5435. Moreover, A. Fuente, J. Cernicharo & A. Omont (1998) detected emission lines of C_2H, C_2H_2 and HCN, and calculated their abundances relative to H_2. Later, L. Začs et al. (2016) detected blue-shifted emission lines of CN and C_2. Recently, Y. Zhang (2020), used the Arizona Radio Observatory 12 m telescope and the Heinrich Hertz Submillimeter Telescope 10 m telescope, and reported the detection about 13 distinct molecular species and their isotopologues in IRAS 22272+5435, including the detection of 10 transitions of HC_3N. In the late stages of stellar evolution, the formation of $HC_{2n+1}N$ ($n = 1, 2, 3, 4$) is driven by a series of reactions involving simpler hydrocarbons and cyano radicals (K. Fukuzawa, Y. Osamura & I. Schaefer 1998; J.-C. Loison, V. Wakelam & K. M. Hickson 2014):

$$C_{2n}H_2 + C_2H \rightarrow C_{2n+2}H_2 + H, \quad (1)$$

$$CN + C_{2n}H_2 \rightarrow HC_{2n+1}N + H. \quad (2)$$

As representative molecules, through experimentally measured reactions, C_2H_2 and C_2H can react with each other to form C_4H_2 (D. Chastaing et al. 1998). Moreover, C_2H_2 can also react with CN to generate HC_3N (D. E. Woon & E. Herbst 1997). This indicates that it is feasible to generate cyanopolyynes using Reactions 1 and 2. Given that HC_3N has been detected in IRAS 22272+5435, it is reasonable to suspect the presence of longer cyanopolyynes (HC_5N, HC_7N, and HC_9N) in the CSE of this source.

To investigate the presence of cyanopolyynes in IRAS 22272+5435, we utilized observations from the Tianma 65 m Radio Telescope (TMRT) and the Purple Mountain Observatory (PMO) 13.7 m MM-Wave Telescope to identify their emission transitions. For HC_5N and HC_7N that were not detected, we constructed a radiative transfer model to simulate their signal intensities.

2 OBSERVATIONS

2.1 The Ku-band observations of TMRT

Our observation of IRAS 22272+5435 was firstly carried out using TMRT, a 65-meter diameter telescope located at the suburbs of Shanghai, China. The telescope has eight receiver systems, among which the Ku-band receiver is a dual-beam dual-polarization cryogenic receiver (LCP and RCP) that covers the frequency range of 12–18 GHz. The efficiency of the Ku-band receiver can reach about 60 per cent at moderate elevations, with a system-equivalent flux density of approximately 38 Jy. The half-power beamwidth (HPBW) of TMRT at ∼15 GHz is ∼ 53 arcsec. The receiver noise temperature ranges between 10–30 K, and the system noise temperature is around

Table 1. The parameters of molecular transitions expected to be observed using TMRT and the PMO 13.7 m MM-Wave Telescope.

Specie	Transition	Rest freq. (MHz)	$S\mu^2$ (D^2)	E_u/k (K)	Telescope
HC_5N	$J = 5$–4	13 313.31	281.2266	1.916 87	TMRT
HC_9N	$J = 27$–26	15 687.92	2190.0254	10.540 55	TMRT
HC_7N	$J = 14$–13	15 791.99	975.8618	5.684 24	TMRT
HC_5N	$J = 6$–5	15 975.97	337.4518	2.683 59	TMRT
HC_9N	$J = 30$–29	17 431.01	2433.8087	12.966 52	TMRT
HC_7N	$J = 16$–15	18 047.97	1115.2086	7.362 35	TMRT
HC_3N	$J = 2$–1	18 196.23	27.8543	1.309 94	TMRT
HCN	$J = 1$–0	88 631.60	26.8217	4.253 62	PMO 13.7 m
HC_3N	$J = 10$–9	90 979.02	139.2544	24.014 82	PMO 13.7 m

Table 2. The parameters of the spectral lines observed using TMRT and the PMO 13.7 m MM-Wave Telescope.

Specie	Transition	RMS Noise (mK)	v_{LSR} (km s^{-1})	Δv (km s^{-1})	ΔT_{mb} (mK)	$\int T_{mb} dv$ (K km s^{-1})	N_{tot} (cm^{-2})	f_X
HC_5N	$J = 5$–4	4.2	–	–	–	< 0.063	$< 1.4 \times 10^{15}$	$< 2.0 \times 10^{-8}$
HC_9N	$J = 27$–26	4.3	–	–	–	< 0.064	$< 2.1 \times 10^{15}$	$< 3.6 \times 10^{-8}$
HC_7N	$J = 14$–13	4.2	–	–	–	< 0.063	$< 2.1 \times 10^{15}$	$< 3.6 \times 10^{-8}$
HC_5N	$J = 6$–5	4.1	–	–	–	< 0.061	$< 7.8 \times 10^{14}$	$< 1.4 \times 10^{-8}$
HC_9N	$J = 30$–29	4.7	–	–	–	< 0.070	$< 1.9 \times 10^{15}$	$< 3.3 \times 10^{-8}$
HC_7N	$J = 16$–15	4.9	–	–	–	< 0.073	$< 1.9 \times 10^{15}$	$< 3.3 \times 10^{-8}$
HC_3N	$J = 2$–1	4.5	–	–	–	< 0.067	$< 2.6 \times 10^{15}$	$< 4.5 \times 10^{-8}$
HCN	$J = 1$–0	7.2	−25.2(0.1)	13.4(0.3)	143.1	2.047(0.039)	5.6×10^{15}	1.0×10^{-7}
HC_3N	$J = 10$–9	9.1	−30.0(0.6)	13.6(1.1)	38.7	0.562(0.044)	1.4×10^{15}	2.4×10^{-8}

40 K when the telescope points towards the zenith (J.-P. Wang, L.-F. Yu & R.-B. Zhao 2016). During summer, the high water vapor content in the atmosphere and the deformation caused by sunlight increase the instability of most receivers. However, the Ku-band receiver is less affected (J. Q. Wang et al. 2017), making it a suitable choice for this observation.

The observations were made on 2023 November 23 (UTC), targeting IRAS 22272+5435 (J2000 coordinates: $22^h29^m10^s.30$, $+54°51'06''.30$). We used the digital back-end system (J. Li et al. 2016) to record the data. This system offers 29 observational modes, and we selected mode 2 for our observations. Each bank has a bandwidth of 1.5 GHz and can operate independently. In mode 2, each bank has 16 384 channels, resulting in a frequency resolution of $\sim$ 91.553 kHz, corresponding to a velocity resolution of $\sim$ 1.83 km s^{-1} at 15 GHz. For this observation, IRAS 22272+5435 was scanned 90 times, with each scan consisting of 1.5 min of integration at the source and 1.5 min of integration at the off source. The effective observation times were 4.53 h. The parameters of the molecular transitions we observed in this study are listed in Table 1, which were taken from the Splatalogue data base[1] (A. Remijan & A. Markwick-Kemper 2007) except for the rest frequency. Rest frequencies are based on the data recorded in CDMS (H. S. Müller et al. 2001, 2005).

2.2 The observations of PMO 13.7 m MM-Wave Telescope

We subsequently conducted further observations of IRAS 22272+5435 using the PMO 13.7 m MM-Wave Telescope located in Delingha, Qinghai Province, China, at a higher frequency of around 90 GHz. The observations were carried out on 2024 May 16 and 27 (UTC). The system temperature of the telescope ranges between 150–300 K (J. Li et al. 2013), with a pointing accuracy for celestial targets of $\lesssim$ 5 arcsec (Y. Su et al. 2019). The receiver front-end utilizes a nine-beam sideband separation Superconduction Spectroscopic Array Receiver system, while the back-end employs a high-resolution Fast Fourier Transform Spectrometer (FFTS) to record spectral data. Each FFTS has a bandwidth of 1 GHz with 16 384 channels, providing a frequency resolution of ∼61 kHz (W. Shan et al. 2012). For each scan, both the on- and the off-source integration times were 30 s, resulting in an effective observation time of $\sim$ 4.1 h, including the telescope's movement time. The main beam efficiency of the telescope is $\sim$ 60 per cent[2], with an HPBW of $\sim$ 51 arcsec at 90 GHz and a velocity resolution of $\sim$ 0.2 km s^{-1}. The parameters of the molecular transitions we observed in this study are also listed in Table 1.

3 RESULTS

3.1 The overall observations

In reducing the data, the gildas/class[3] package was used. All spectra were derived through subtraction of a linear baseline. The velocity data are given relative to the local standard of rest (LSR). Furthermore, all molecular lines were smoothed to improve the signal-to-noise ratio (SNR) for individual channels.

Observations using TMRT covered one transition of HC_3N, two transitions of HC_5N, two transitions of HC_7N, and two transitions of HC_9N. Table 2 lists the results. The root mean square (RMS) noise obtained after the baseline adjustment is also listed in the table,

[1] www.splatalogue.net

[2] http://www.radioast.nsdc.cn/zhuangtaibaogao.php

[3] https://www.iram.fr/IRAMFR/GILDAS/

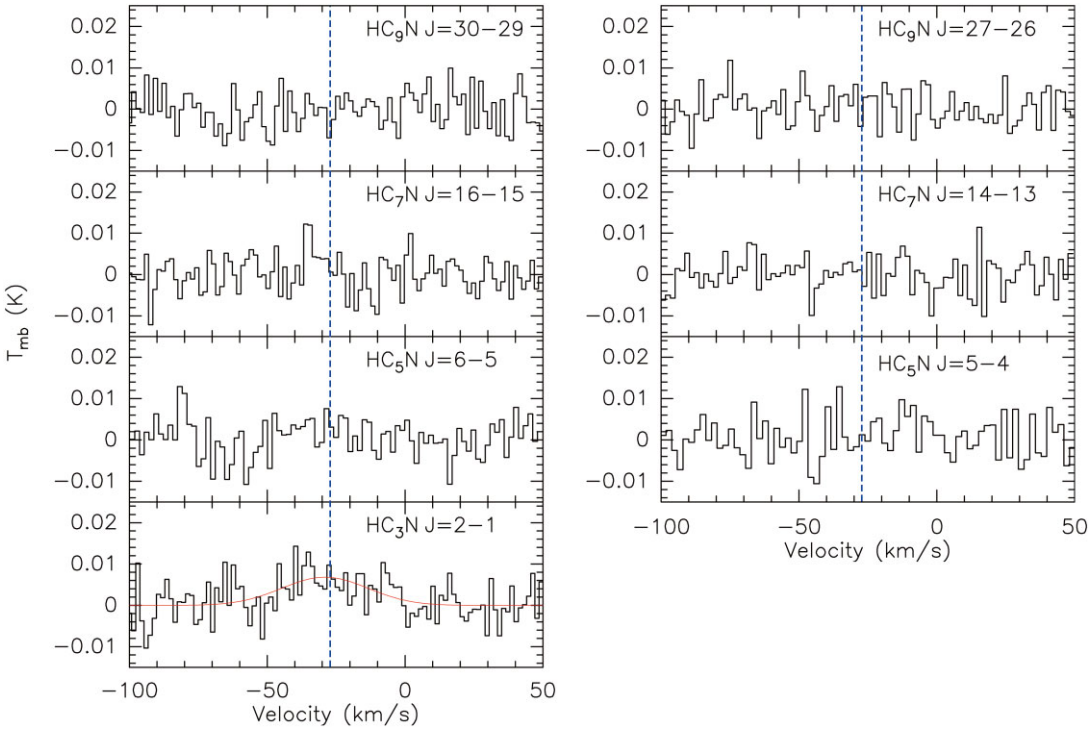

Figure 1. Observational results of HC_3N, HC_5N, HC_7N, and HC_9N using TMRT. The dashed line represents the position of $v_{LSR} = -28.1\,km\,s^{-1}$. The Gaussian fitting result of HC_3N $J = 2$–1 is marked with a line.

with all RMS noise values ranging between 4 and 5 mK. Based on previous observations of the CO molecule in IRAS 22272+5435, we assume a system velocity of $v_{LSR} = -28.1\,km\,s^{-1}$ (J.-i. Nakashima et al. 2012). Fig. 1 shows the observational results from TMRT. For the HC_3N $J = 2$–1 transition, there appears to be a significant signal in the range of -50 to $0\,km\,s^{-1}$. Fitting the spectrum in this region, the peak signal intensity (ΔT_{mb}) is 6.808 mK. Compared to the RMS noise of 4.545 mK, the signal does not reach the 3σ significance level. For the HC_7N $J = 16$–15 transition, a significant signal is detected in the range of -36 to $-27\,km\,s^{-1}$, with an RMS noise of 4.921 mK. ΔT_{mb} reaches a 3σ significance level. However, considering that we did not observe HC_5N, which should theoretically be more easily detected, and given the narrow line width of the signal whose offset relative to v_{LSR} of the source, we tend to believe that this is not the signal of HC_7N $J = 16$–15. For the other transitions we aimed to detect, the observational results do not show significant line widths. Therefore, no signal is expected at $v_{LSR} = -28.1\,km\,s^{-1}$, indicating that we did not detect any transition signals from these molecules.

In contrast, the observations using the PMO 13.7 m MM-Wave Telescope successfully confirmed the HC_3N $J = 10$–9 transition, consistent with earlier reports. By comparing the rest frequencies of the lines from the Splatalogue data base, we confirmed the HCN $J = 1$–0 and HC_3N $J = 10$–9 transitions, with rest frequencies of 88631.60 and 90979.02 MHz, respectively. The line of HCN $J = 1$–0 reveals the hyperfine structure. We used the Gaussian function to fit HCN $J = 1$–0 and the SHELL function to fit HC_3N $J = 10$–9, and the relevant line parameters are listed in Table 2. As shown in Fig. 2, very strong molecular signals are present at $v_{LSR} = -28.1\,km\,s^{-1}$, with a much higher significance than 3σ. The full width at half maximum (Δv or FWHM) of these two signals of $\sim 13.5\,km\,s^{-1}$, is consistent with the FWHM of multiple CO transitions observed in IRAS 22272+5435 using several telescopes (M. R. Schmidt et al. 2013).

The detection of the HC_3N $J = 10 - 9$ transition by the PMO 13.7 m MM-Wave Telescope was not unexpected, as multiple transitions of HC_3N have already been detected in IRAS 22272+5435 (Y. Zhang 2020; J.-J. Qiu et al. 2024). However, most of the currently detected HC_3N transitions are concentrated in the high-frequency range above 80 GHz, corresponding to higher J values. For the low-frequency range below 20 GHz, it seems that the HC_3N $J = 2$–1 transition was detected with an extremely low SNR. When compared with the ten HC_3N transitions reported by Y. Zhang (2020) in the rotational diagram (see Fig. 3), the data point for the suspected $J = 2$–1 transition in this study deviates significantly from the fitted line. Moreover, the FWHM of this signal is relatively large and shows notable differences from the HC_3N lines detected by Y. Zhang (2020) and the PMO 13.7 m MM-Wave Telescope. Therefore, we are inclined to conclude that no HC_3N signal was detected by TMRT below 20 GHz.

3.2 Estimation of column density and fractional abundance

To obtain the column densities (N_{tot}) of observed molecular lines and further estimate molecular fractional abundances, we employed a method commonly used for standard rotation diagram analysis. Assuming that the excitation of spectral lines satisfies the local thermodynamic equilibrium (LTE) approximation, ignoring the cosmic microwave background radiation, and all transitions are optically thin and satisfy the Rayleigh–Jeans approximation, N_{tot} and excitation temperature (T_{ex}) of lines can be derived from the following equation (B. E. Turner 1989):

$$\ln\frac{N_u}{g_u} = \ln\frac{3kW}{8\pi^3\nu S\mu^2} = \ln\frac{N_{tot}}{Q(T_{ex})} - \frac{E_u}{kT_{ex}}, \quad (3)$$

where, N_u is the population, g_u is statistical weights of the upper energy level, k is the Boltzmann constant, W is the integral of the

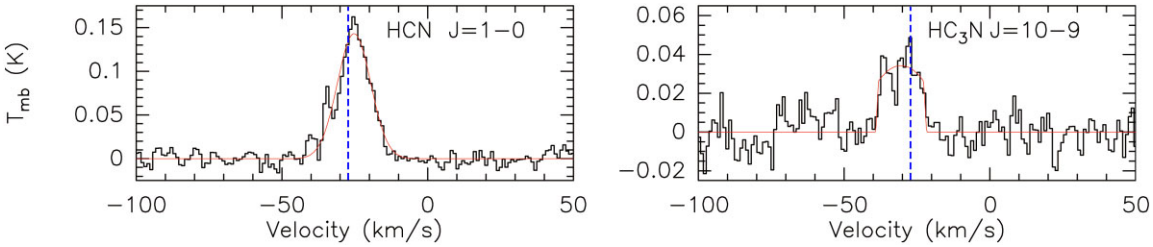

Figure 2. Observational results of HCN and HC_3N using the PMO 13.7 m MM-Wave Telescope. The signals of HCN $J = 1$–0 and HC_3N $J = 10$–9 are fitted using Gaussian and SHELL functions, respectively. The fitting curves obtained by fitting the transition signals are shown, with dashed lines represent the positions of $v_{LSR} = -28.1$ km s^{-1}.

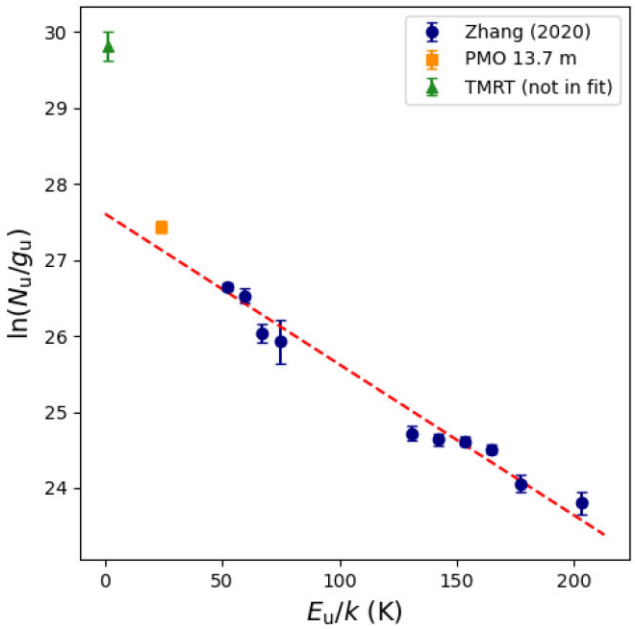

Figure 3. Rotational diagram based on the ten HC_3N transitions detected by Y. Zhang (2020) and the HC_3N $J = 10$–9 transition detected by PMO 13.7 m MM-Wave Telescope (in the fit). The data point of the suspected HC_3N $J = 2$–1 transition (from TMRT) is plotted only as an upper limit due to its low SNR and is not included in the fit.

source brightness temperature (T_R) with respect to velocity, ν is the rest frequency of the line, and Q, is the partition function related to T_{ex}, which can be found in the Splatalogue database.

In practical observations, molecular signals often cannot fill the beam of a telescope, so we need to introduce a beam dilution factor η_{BD}:

$$\eta_{BD} = \frac{\theta_S^2}{\theta_S^2 + \theta_{beam}^2}, \tag{4}$$

where θ_{beam} is the HPBW of the antenna and θ_S is the source size, which varies depending on species. For the AGB source IRC+10216, the emission region of the CO $J = 2$–1 transition has a diameter of $\sim 80''$ (J. Cernicharo et al. 2015), while that of the HC_3N $J =$ 16–15 transition is ~ 30 arcsec (P. Audinos, C. Kahane & R. Lucas 1994). Based on this reference, and considering that J.-i. Nakashima et al. (2012) measured the CO $J = 2$–1 emission region in IRAS 22272+5435 to be ~ 8 arcsec in diameter, we here simply adopted a θ_S value of $3''$. In this way, we can establish a relationship between T_R and the main beam brightness temperature (T_{mb}):

$$T_R = \frac{T_{mb}}{\eta_{BD}}. \tag{5}$$

Typically, rotational diagram analysis requires us to detect at least two transitions of a molecule within a certain frequency interval. However, in this study, we only detected one transition of each of the HCN and HC_3N molecules. We incorporated the HC_3N $J = 10$–9 transition observed at PMO 13.7 m MM-Wave Telescope and the 10 HC_3N transitions observed by Y. Zhang (2020) into the rotational diagram fitting, resulting in a T_{ex} of 50.4 K. (see Fig. 3). Therefore, we assumed that T_{ex} of HCN and HC_3N is 50.4 K. Using the molecular column density, we can calculate the fractional abundance (f_X) of these molecules relative to H_2, which requires knowledge of the H_2 column density. However, so far, no relevant studies have reported detections of H_2 emission lines in IRAS 22272+5435. The few attempts to detect H_2 in this source have all ended in failure (e.g. C. J. Davis et al. 2003). Fortunately, we can still calculate the column density of H_2 (N_{H_2}) estimated by using equation (6) (Y. Gong et al. 2015):

$$N_{H_2} = \frac{\dot{M}}{\pi R v_{exp} \mu m_H}. \tag{6}$$

Here, $\dot{M}$ is the stellar mass-loss rate, which for IRAS 22272+5435 is $\sim 3.5 \times 10^{-4}$ $M_\odot$ yr^{-1} (A. Mishra et al. 2016); R is the molecular emission radius, which we assume to be the same as the HC_3N envelope radius of 1.5 arcsec; v_{exp} is the gas expansion velocity, we assume this value to be 8.5 km s^{-1}, consistent with M. R. Schmidt et al. (2013); μ is the average mass of gas particles, which can be taken as 2.3 amu for a gas primarily composed of H_2 (S. Massalkhi et al. 2018); m_H is the mass of a hydrogen atom. We calculated a column density of 5.8×10^{22} cm^{-2} for H_2. Then, we need to divide the molecular column density by the H_2 column density to obtain the molecular fractional abundance relative to H_2:

$$f_X = \frac{N_X}{N_{H_2}}. \tag{7}$$

For HCN $J = 1$–0 and HC_3N $J = 10$–9, we used the aforementioned methods to calculate their column densities and fractional abundances. The results are shown in Table 2. As for the molecular transitions that were not observed in Figs 1 and 3, we estimated their upper limits on column densities and fractional abundances using the detected RMS noise. A 3σ level was adopted as the detection threshold, assuming that any signal above this level is considered significant. Furthermore, we assumed that the line widths of the undetected molecular transitions are close to those of the detected lines of HCN and HC_3N ($\sim$13.5 km s^{-1}). The upper limit for the integrated intensity was calculated by $3\sigma \frac{\Delta v}{\sqrt{n}}$ (Y. Zhang et al. 2008), where Δv is the assumed line width and n is the channel number

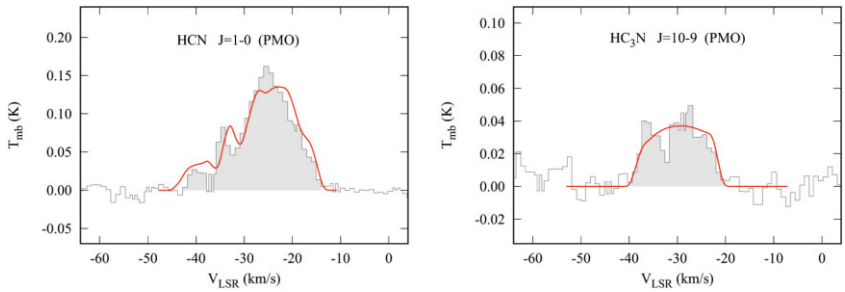

Figure 4. Simulated profiles of HCN $J = 10$–9 and HC_3N $J = 10$–9 in IRAS 22272+5435 if we used the PMO 13.7 m MM-Wave Telescope to observe. The shadowed lines represent the observed transitions.

within the Δv. For TMRT, the value of n is ∼7.37. Using equations (2) and 5, we estimated the upper limits on the column densities and fractional abundances, with the results summarized in Table 2. It is worth noting that the column densities and fractional abundances of HC_3N and HCN derived by Y. Zhang (2020) show a difference of an order of magnitude compared to the results of this study. One possible reason is that Y. Zhang (2020) assumed a larger source size (5″), which may have led to lower calculated values of column density and fractional abundance.

4 RADIATIVE TRANSFER CALCULATIONS

Our observations detected only the HC_3N $J = 10$–9 transition, while heavier cyanopolyynes were not detected. The assumption of a spherically symmetric molecular envelope is supported by previous interferometric studies showing that the envelope of IRAS 22272+5435 appears roughly spherical at large scales, with no clear evidence of fast bipolar outflows (R. Neri et al. 1998; V. Bujarrabal et al. 2001). Although T. Ueta et al. (2001) revealed small-scale structures in scattered light images, these do not significantly affect the large-scale molecular distribution considered in our radiative transfer modelling. To determine whether these molecules might exist in IRAS 22272+5435, we used a radiative transfer model to simulate the expected signal intensities for HC_3N, HC_5N, and HC_7N lines that could potentially be observed with TMRT.

We used the numerical code MOLEXCSE for line emission modelling, as described in detail in M. R. Schmidt et al. (2016). MOLEXCSE is suitable for spherical envelopes with arbitrary velocity fields under non-LTE conditions. For cyanopolyynes, the molecular models do not include infrared pumping. The input files were constructed using molecular structure data from the CDMS data base, covering all energy levels below $J = 60$ for HC_5N and HC_7N, while the HC_3N model was downloaded from the LAMBDA data base[4] (F. L. Schöier et al. 2005), which includes hyperfine structure. For HC_3N alone, we adopted collisional de-excitation rates by para- and ortho-H_2 calculated by A. Faure, F. Lique & L. Wiesenfeld (2016), while for heavier molecules, we adopted the approximate method proposed by S. Deguchi & M. Uyemura (1984). Due to the lack of theoretical and successfully observed data for HC_9N, we did not simulate line profiles of HC_9N.

We first simulated the signal intensities for cyanopolyynes observed in IRC+10216 using the Effelsberg 100 m radio telescope, comparing these with observational data from Y. Gong et al. (2015) to calibrate and test the model (see the appendix). After determining the cyanopolyynes' distributions in the C-rich AGB star IRC+10216, we extrapolated this model to the post-AGB star IRAS 22272+5435. The reason behind this approach is that we assume that emission lines of cyanopolyynes originate in the photodissociation region of the AGB remnant of IRAS 22272+5435, in a quite analogous way to that of IRC+10216. The distributions of HC_3N and heavier cyanopolyynes were based on the abundance distributions derived for IRC+10216. The distance from IRAS 22272+5435 was set at 1.67 kpc, adopted by M. R. Schmidt et al. (2013), but slightly lower than the distance observed by *Gaia* (D. Kamath et al. 2022). The peak of the HC_3N spatial distribution was adjusted to match the maximum value of the HC_3N $J = 10$–9 signal observed with the PMO 13.7 m MM-Wave Telescope (see the right panel of Fig. 4), using an HPBW of 50.6 arcsec.

In addition, we have simulated the emission profile of the three hyperfine components of the HCN $J = 1$–0 transition. For this purpose, we used the HCN model from the LAMBDA data base, neglecting infrared pumping effects. The photodissociation radius of HCN adopted in our model is taken directly from M. R. Schmidt et al. (2013), who derived it based on a multitransition CO and HCN analysis. This defines the outer boundary of the HCN envelope used in our modelling. The fit is shown in the left panel of Fig. 4. The distribution of HCN was taken from M. R. Schmidt et al. (2013) (see the purple line in Fig. 5).

The CSE model for IRAS 22272+5435 was adopted from M. R. Schmidt et al. (2013), derived from analyses of CO transitions observed with ground-based radio telescopes and Herschel/HIFI (up to $J = 10$–9). The temperature structure, shown as the blue curve in Fig. 5, was obtained from CO low-J transition analysis by M. R. Schmidt et al. (2013). This thermal structure model was computed from first principles, including dust-gas collisional heating, photoelectric heating, and molecular cooling processes. In particular, the analysis of the rotational diagram by Y. Zhang (2020) indicated an excitation temperature of 54 ± 3 K for HC_3N based on ten transitions, completely consistent with the estimated gas temperature of IRAS 22272+5435 (M. R. Schmidt et al. 2013). The expansion velocity is a well-constrained parameter, remaining constant within the region of interest ($v_{\rm exp} = 8.5\,{\rm km\,s^{-1}}$). The H_2 gas density distribution was determined from the mass-loss rate prescription given in M. R. Schmidt et al. (2013) and the mass conservation equation. Turbulent velocity calculations followed the method of M. R. Schmidt et al. (2013).

According to our calculations, the peak abundance of HC_3N is 5.9×10^{-7}, peak abundances of HC_5N and HC_7N were scaled relative to HC_3N to agree with the ratios calculated in IRC+10216 (1 : 0.47 : 0.17 for HC_3N: HC_5N: HC_7N). Abundance distributions are presented in the upper panel of Fig. 5 with the scale on the right side. The calibrated model of the distribution of cyanopolyynes in

[4]https://home.strw.leidenuniv.nl/~moldata/

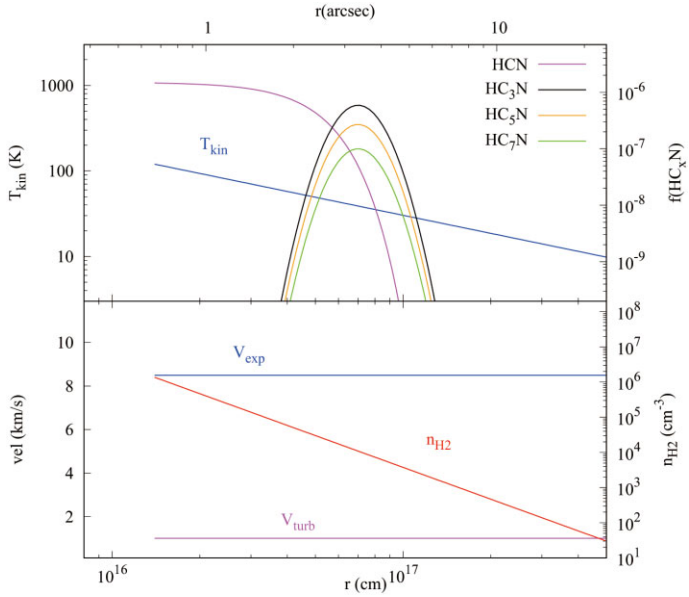

Figure 5. The physical parameters of the model of the outer envelope of IRAS 22272+5435 assumed in modelling of $HC_{2n+1}N$ ($n = 1, 2, 3$) lines. The gas kinetic temperature distribution was obtained from CO low-J transition analysis by M. R. Schmidt et al. (2013). The abundance distributions of HCN, HC_3N, HC_5N, and HC_7N are shown on the top panel, where the abundance distribution functions of HC_3N, HC_5N, and HC_7N exhibit Gaussian functions. The H_2 gas density distribution was determined from the mass-loss rate prescription given in M. R. Schmidt et al. (2013) and the mass conservation equation. Turbulent velocity calculations followed the method of M. R. Schmidt et al. (2013). The expansion velocity is 8.5 km s^{-1}.

the AGB remnant of IRAS 22272+5435 has been used to predict the intensities of $HC_{2n+1}N$ transitions to be observed by TMRT, as shown in Fig. 6. No radiative pumping was included in calculations, hence neglecting infrared pumping in our radiative transfer modelling implies that a higher abundance of HC_3N is required to reproduce the observed emission. Therefore, the derived HC_3N column density and fractional abundance represent upper limits; inclusion of infrared pumping would reduce the required molecular abundance. As shown in Section 3.2, the excitation temperature (50.4 K) derived from 11 transitions of HC_3N is in good agreement with the gas kinetic temperature estimated by M. R. Schmidt et al. (2013). This indicates that the lines are close to thermalization, supporting our assumption that infrared pumping can be reasonably neglected in the non-LTE calculations. Consequently, the derived column densities and abundances are not expected to significantly overestimate the actual values.

5 DISCUSSION

In this study, the HC_3N $J = 10$–9 transition detected with the PMO 13.7 m MM-Wave Telescope in IRAS 22272+5435 has a peak T_{mb} of ∼0.04 K, which is significantly lower than the peak T_{mb} (∼2.5 K) of the same transition detected in IRC+10216 with the same telescope (J. Tuo et al. 2024). For the larger molecules HC_5N, HC_7N, and HC_9N, we did not detect any significant signals. However, our model calculations show that the peak abundances of HC_3N, HC_5N, and HC_7N in IRAS 22272+5435 (see Fig. 5) are of the same order of magnitude as those of these molecules in IRC+10216 (see Fig. A1 in the appendix). Considering that there have been multiple successful observation records of HC_5N and HC_7N in IRC+10216 at present (e.g. Y. Gong et al. 2015; J. R. Pardo et al. 2022), we believe that the non-detection of HC_5N and HC_7N in IRAS 22272+5435 is unlikely to be due to their low abundances leading to weak emissions.

The distance of IRC+10216 is 130 pc (K. M. Menten et al. 2012), which is much closer to us compared to IRAS 22272+5435 (1.65 kpc). As a result, the received radiation flux from IRAS 22272+5435 is significantly lower, leading to weaker spectral line signals and affecting the detection sensitivity. This is expected to cause the HC_3N signal in IRAS 22272+5435 to be significantly weaker than that in IRC+10216 and to result in the non-detection of HC_5N, HC_7N, and HC_9N in this study. For single-dish telescopes, more distant sources may require longer integration times to achieve a sufficient SNR. Moreover, as the carbon-chain length increases, the transition frequencies of cyanopolyynes for the same J value decrease. This results in a larger beam dilution factor for the telescope when detecting these transitions, also requiring longer observation times to reduce noise and distinguish molecular transition signals from the background noise. While observations at fixed J values lead to larger beam dilution for heavier cyanopolyynes due to their lower transition frequencies, an alternative strategy is to observe transitions at similar frequencies. Larger molecules have more closely spaced rotational levels, making it possible to select transitions near the 90 GHz frequency of HC_3N $J = 10$–9. In this case, the beam size remains approximately constant, and the key limiting factor becomes the larger partition function of heavier molecules, which weakens the line intensity. According to our simulations, detecting the HC_5N $J = 6$–5 transition at a 3σ significance level with TMRT would require an observation time of 43 h, nearly ten times the observation duration of this study.

6 SUMMARY

This study investigates the presence of cyanopolyynes ($HC_{2n+1}N$, where $n = 1, 2, 3, 4$) in the CSE of the C-rich post-AGB star IRAS 22272+5435 using observations from TMRT and the PMO 13.7 m MM-Wave Telescope. The observations with the PMO 13.7 m MM-Wave Telescope successfully detected the HC_3N $J = 10$–9 transition

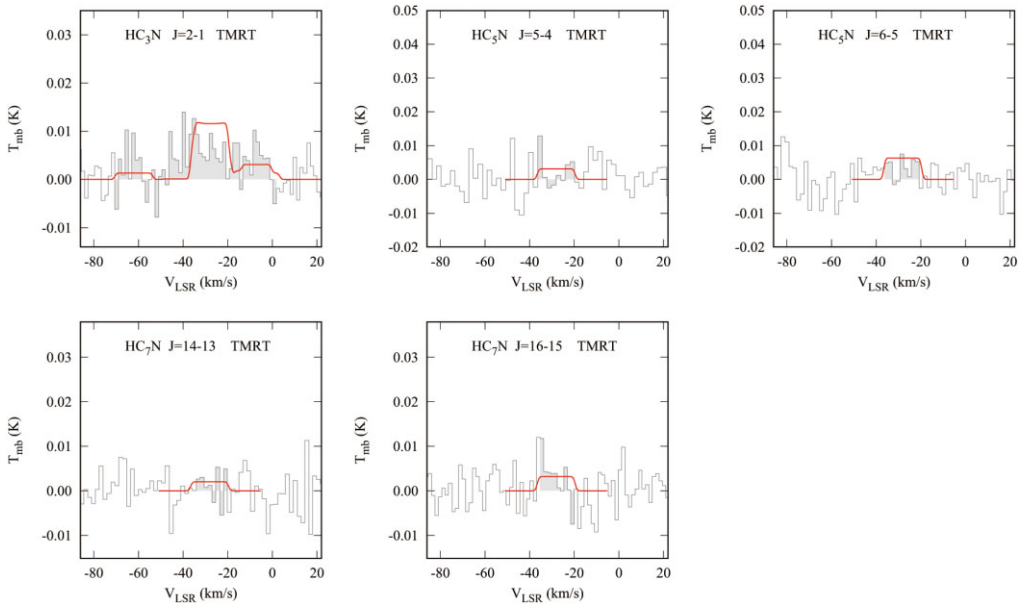

Figure 6. Simulated profiles of selected transitions of HC_3N, HC_5N, and HC_7N in IRAS 22272+5435 if we use TMRT to observe. HC_3N $J = 2$–1 transition contains hyperfine structure. The HPBWs used in the calculations are 53, 61, and 61 arcsec, respectively, for HC_3N, HC_5N and HC_7N. The grey line represents the observational results.

and the HCN $J = 1 - 0$ transition, while no cyanopolyynes were detected with TMRT. Consequently, the HC_5N, HC_7N, and HC_9N column density upper limits and abundance upper limits were estimated through LTE calculations.

A radiative transfer model was used to simulate the emission of cyanopolyynes, calibrated against data from the AGB star IRC+10216. According to our modelling results, the simulated profiles of HCN $J = 1$–0 and HC_3N $J = 10$–9 matches well with the data observed by the PMO 13.7 m MM-Wave Telescope. The modelling results suggest that HC_5N and HC_7N may be present in the envelope of IRAS 22272+5435; however, due to a large distance for IRAS 22272+5435, and the low observing frequencies, significant beam dilution effects make the detection challenging under the current observational conditions. Calculations indicate that detecting the HC_5N $J = 6$–5 transition with a 3σ signal using TMRT would require an integration time of up to 43 h, far exceeding the duration of the current observations.

This study confirms the presence of HC_3N in the CSE of the post-AGB star and provides important insights for future, more sensitive observations of heavier cyanopolyynes. The HC_3N abundance in IRAS 22272+5435 is found to be comparable in order of magnitude to that in IRC+10216, suggesting that similar carbon-chain growth chemistry may be occurring in its envelope. Future deep observations with higher sensitivity instruments will help to further uncover the formation and evolutionary processes of complex organic molecules in post-AGB stars.

ACKNOWLEDGEMENTS

We are extremely grateful to the anonymous reviewer for the fruitful and insightful comments, along with valuable inputs to this manuscript, which greatly helped improve the quality of this paper. Xiaohu Li acknowledges support from the National Science Foundation of China (No. 12473025), the Natural Science Foundation of Xinjiang Uygur Autonomous Region (No. 2024D01E37), and the Chinese Academy of Sciences "Light of West China" Program (No. xbzg-zdsys-202410). Tom J. Millar thanks the United Kingdom Science and Technology Facilities Council for support through grant ST/T000198/1. Gleb Fedoseev, Jixing Ge, Wasim Iqbal, and Yihan Wu thank the Xinjiang Tianchi Talent Program (2024). Yong Zhang, Chuanlu Yang, Tao Yang, and Xuan Fang thank the Xinjiang Tianchi Talent Program (2023). Xia Zhang thanks the National Natural Science Foundation of China under grant 12203091. This work also received the support of the Natural Science Foundation of Xinjiang Uygur Autonomous Region (No. 2025D01D49, 2025D01B174, 2025D01B172, 2022D01B221).

DATA AVAILABILITY

The data will be shared on reasonable request to the corresponding author.

REFERENCES

Audinos P., Kahane C., Lucas R., 1994, A&A, 287, L5
Bujarrabal V. et al., 2012, A&A, 537, A8
Bujarrabal V., Castro-Carrizo A., Alcea J., Sánchez Contreras C., 2001, A&A, 377, 868
Cernicharo J., Cabezas C., Agúndez M., Endo Y., Tercero B., Marcelino N., de Vicente P., 2024, A&A, 686, L15
Cernicharo J., Goicoechea J. R., Caux E., 2000, ApJ, 534, L199
Cernicharo J., Marcelino N., Agúndez M., Guélin M., 2015, A&A, 575, A91
Cernicharo J., Marcelino N., Pardo J. R., Agúndez M., Tercero B., de Vicente P., Cabezas C., Bermúdez C., 2020, A&A, 641, L9
Chastaing D., L. James P., R. Sims I., W. M. Smith I., 1998, Faraday Discuss., 109, 165
Davis C. J., Smith M. D., Stern L., Kerr T. H., Chiar J. E., 2003, MNRAS, 344, 262
De Beck E. et al., 2012, A&A, 539, A108
De Beck E., Decin L., de Koter A., Justtanont K., Verhoelst T., Kemper F., Menten K. M., 2010, A&A, 523, A18
Deguchi S., Uyemura M., 1984, ApJ, 285, 153
Faure A., Lique F., Wiesenfeld L., 2016, MNRAS, 460, 2103

Fedoseev G., Li X., Baratta G. A., Palumbo M. E., Chuang K. J., 2025, A&A, 693, A277
Fuente A., Cernicharo J., Omont A., 1998, A&A, 330, 232
Fukuzawa K., Osamura Y., Schaefer Henry F. I., 1998, ApJ, 505, 278
Gong Y., Henkel C., Spezzano S., Thorwirth S., Menten K. M., Wyrowski F., Mao R. Q., Klein B., 2015, A&A, 574, A56
Hrivnak B. J., Kwok S., 1991, ApJ, 371, 631
Hrivnak B. J., Lu W., Sperauskas J., Van Winckel H., Bohlender D., Začs L., 2013, ApJ, 766, 116
Kamath D., Van Winckel H., Ventura P., Mohorian M., Hrivnak B. J., Dell'Agli F., Karakas A., 2022, ApJ, 927, L13
Kwok S., 1993, ARA&A, 31, 63
Li J. et al., 2016, ApJ, 824, 136
Li J., Wang J. Z., Gu Q. S., Zheng X. W., 2013, A&A, 555, A18
Loison J.-C., Wakelam V., Hickson K. M., 2014, MNRAS, 443, 398
Massalkhi S. et al., 2018, A&A, 611, A29
McCarthy M. C. et al., 2021, Nat. Astron., 5, 176
McGuire B. A. et al., 2021, Science, 371, 1265
Menten K. M., Reid M. J., Kamiński T., Claussen M. J., 2012, A&A, 543, A73
Millar T. J., Herbst E., 1994, A&A, 288, 561
Mishra A., Li A., Jiang B. W., 2016, ApJ, 825, 68
Müller H. S. P., Thorwirth S., Roth D. A., Winnewisser G., 2001, A&A, 370, L49
Müller H. S., Schlöder F., Stutzki J., Winnewisser G., 2005, J. Mol. Struct., 742, 215
Nakashima J.-i., Koning N., Volgenau N. H., Kwok S., Yung B. H. K., Zhang Y., 2012, ApJ, 759, 61
Neri R., Kahane C., Lucas R., Bujarrabal V., Loup C., 1998, A&AS, 130, 1
Olofsson H., 1996, Ap&SS, 245, 169
Pardo J. R. et al., 2022, A&A, 658, A39
Qiu J.-J. et al., 2024, AJ, 167, 91
Reddy B. E., Lambert D. L., Gonzalez G., Yong D., 2002, ApJ, 564, 482
Remijan A., Markwick-Kemper A., 2007, Bull. Am. Astron. Soc., 39, 963
Schmidt D. R., Ziurys L. M., 2019, ApJ, 881, L38
Schmidt M. R. et al., 2016, A&A, 592, A131
Schmidt M. R., Začs L., Pułecka M., Szczerba R., 2013, A&A, 556, A46
Schöier F. L., van der Tak F. F. S., van Dishoeck E. F., Black J. H., 2005, A&A, 432, 369
Shan W. et al., 2012, IEEE Trans. Terahertz Sci. Technol., 2, 593
Su Y. et al., 2019, ApJS, 240, 9
Szczerba R., Omont A., Volk K., Cox P., Kwok S., 1997, A&A, 317, 859
Szczerba R., Siódmiak N., Stasińska G., Borkowski J., 2007, A&A, 469, 799
Thaddeus P., McCarthy M., 2001, Spectrochim. Acta Part A: Mol. Biomol. Spectrosc., 57, 757
Truong-Bach, Graham D., Nguyen-Q-Rieu, 1996, A&A, 312, 565
Tuo J. et al., 2024, ApJS, 271, 45
Turner B. E., 1989, ApJS, 70, 539
Ueta T. et al., 2001, ApJ, 557, 831
Van Winckel H., 2003, ARA&A, 41, 391
Wang J. Q. et al., 2017, AcASn, 58, 37
Wang J.-P., Yu L.-F., Zhao R.-B., 2016, IEEE International Conference on Microwave and Millimeter Wave Technology, 1, 6
Wenzel G. et al., 2024, Science, 386, 810
Woon D. E., Herbst E., 1997, ApJ, 477, 204
Xue C. et al., 2020, ApJ, 900, L9
Začs L., Klochkova V. G., Panchuk V. E., 1995, MNRAS, 275, 764
Začs L., Musaev F., Kaminsky B., Pavlenko Y., Grankina A., Sperauskas J., Hrivnak B. J., 2016, ApJ, 816, 3
Zhang X.-Y., Zhu Q.-F., Li J., Chen X., Wang J.-Z., Zhang J.-S., 2017, A&A, 606, A74
Zhang Y., 2020, ApJ, 898, 151
Zhang Y., Kwok S., Dinh-V-Trung, 2008, ApJ, 678, 328
Ziurys L. M., 2006, PNAS, 103, 12274

APPENDIX A: SUPPORTING MODEL CALCULATIONS FOR IRC+10216

The physical and thermal structures of IRC+10216 were taken from E. De Beck et al. (2012). Cyanopolyynes were assumed to be concentrated in a ring ~ 15 arcsec from the central star, with a Gaussian shape. The peak distribution for lighter molecules was assumed to be closer to the star (see Fig. A1). We modeled HC_3N $J = 2$–1, three transitions of HC_5N ($J = 7$–6 to $J = 9$–8), and all transitions of HC_7N from $J = 16$–15 to $J = 23$–22. During modelling, we adjusted the peak distributions of cyanopolyynes to

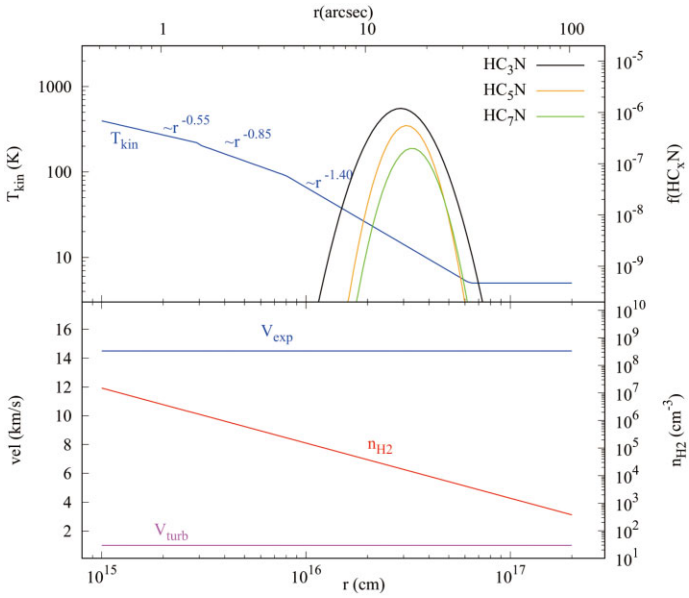

Figure A1. The physical parameters of the model of the outer envelope of IRC+10216 assumed in modelling of $HC_{2n+1}N$ ($n = 1, 2, 3$) lines. The gas kinetic temperature distribution follows parametrization proposed by E. De Beck et al. (2012), adopted for modelling of CO transitions. The distribution of abundances of cyanopolyynes in the form of Gaussian functions are shown on the top panel. The gas number density, which is assumed to be composed of molecular hydrogen is shown on the bottom panel. Assumed turbulent velocity is 1 km s^{-1}, while observed expansion velocity is 14.5 km s^{-1}.

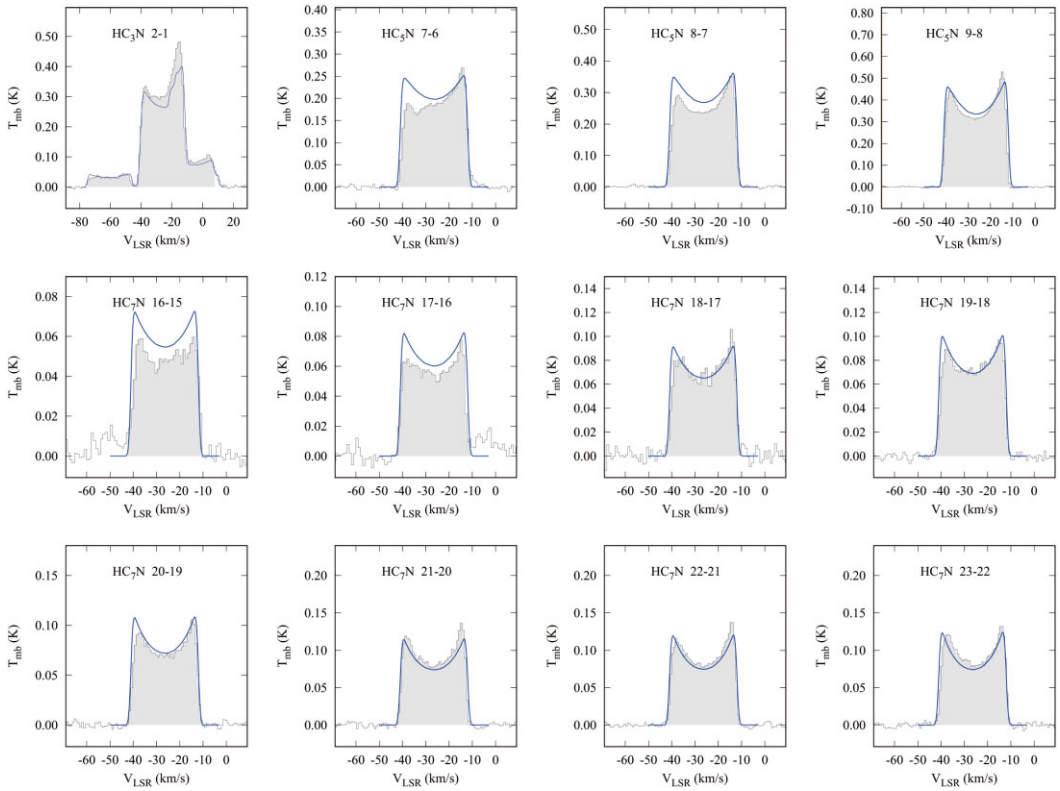

Figure A2. Comparison of HC_3N, HC_5N, and HC_7N spectral lines observed by Y. Gong et al. (2015) in IRC+10216 with simulated profiles from radiative transfer calculations.

match the observations by Y. Gong et al. (2015). The final model results showed good agreement with the observations, as shown in Fig. A2. The results of simulations show that the observations of cyanopolyynes with the Effelsberg telescope are fairly well reproduced. Small asymmetries of line profiles are observed also in ammonia lines (M. R. Schmidt et al. 2016) and are ascribed to the asymmetry of the envelope.

This paper has been typeset from a TEX/LATEX file prepared by the author.